Calculations of Ca adsorption on a MgO(100) surface:
Determination of the binding sites and growth mode

Lijun Xu and Graeme Henkelman

Department of Chemistry and Biochemistry, University of Texas at Austin, Austin, Texas 78712-0165, USA
(Received 7 March 2008; published 2 May 2008)

Density functional theory is used to calculate the adsorption of Ca adatoms on a MgO(100) surface. The Ca monomer binds preferentially to the oxygen site on the terrace with an adsorption energy of 0.84 eV and diffuses by hopping to a nearest neighboring oxygen site with a barrier of 0.45 eV. The binding at F and F^+ oxygen vacancy defects is weaker than on the terrace. Small Ca clusters on the surface are either unstable (dimers and trimers) or very mobile (tetramer). Therefore, a Ca adatom can diffuse around the surface until it reaches a strong-binding site such as a step (2.1 eV), kink (3.9 eV), divacancy (5.5 eV), or even a Mg vacancy (10 eV). When Ca binds to MgO(100), charge is transferred from Ca to the surface. The magnitude of the charge transfer is different between different binding sites, which can help explain the different adsorption energies. The oxygen bound to a step edge can provide a stronger binding for a Ca adatom (7.0 eV), but its existence on MgO(100) still remains to be verified. Based on the adsorption energetics and kinetics, further growth of the Ca particles is expected to occur at strong-binding sites and spread onto the terrace in a three-dimensional growth mode. A two-state kinetic growth model is used to compare our density functional theory calculations with measured heats of adsorption by Zhu *et al.* [J. Am. Chem. Soc. **130**, 2314 (2008)]. This study shows that the defects on MgO(100) have different roles in the growth of alkaline earth metals, such as Ca, as compared to late transition metals, such as Pd.

I. INTRODUCTION

Metal nanoparticles and thin films supported on oxide surfaces have been extensively studied for promising applications in fields such as catalysis, chemical sensing, and fabrication of microelectric and magnetic devices.[1–6] The MgO(100) surface has been a popular substrate in model catalysts due to its simple structure, rigidity with slight rumpling and relaxation, and easy preparation in ultrahigh vacuum (UHV).[7–9] There has been much effort devoted to metal/MgO(100) systems in both experimental and theoretical studies.[1,10–18] One of the key issues is to figure out how and where metal adatoms adsorb and grow on the surface in order to understand the metal-oxide interface and also the MgO(100) surface itself.

On a MgO(100) single crystal, which is either cleaved or grown on a metal support in UHV, there are always defect sites present on the surface.[1,19,20] The defect sites have generally been taken as the main anchoring sites in the nucleation and growth of metal particles or thin films.[1,21,22] The *in situ* atomic force microscope experiment by Barth and Henry found that the UHV-cleaved MgO(100) surface has steps, kinks, adsorbed Mg-O pairs, point defects, and even rectangular pits.[19] Kramer *et al.* applied electron energy loss spectroscopy (EELS) to show that electron sputtering creates neutral oxygen vacancies (F centers) on MgO(100) thin films grown on Ag(100).[23] Sterrer *et al.*[24] applied scanning tunneling microscope and electron paramagnetic resonance on an electron-sputtered MgO(100) surface that was grown on a Mo single crystal.[24] Their results suggest that point defects created on the MgO(100) surface are probably charged oxygen vacancies (F^+ centers) or divacancies and that those point defects can be all over the surface, including at step edges.[24] However, experiments have not been able to identify

the detailed structure of those, especially intrinsic, defect sites.[19,24]

Theoretical calculations can give atomic scale detail of defect sites.[25] Density functional theory (DFT) calculations have shown that oxygen vacancies can be nucleation centers for metal particle growth and divacancy sites can be extremely strong-binding sites.[26] For example, recent studies of Pd island growth on MgO(100) based on DFT calculations indicate that the dominant surface defects should be charged oxygen vacancies or divacancies.[22,27] The important role of point defects has been generally accepted. Both experimental and theoretical studies have focused on transition metals. The conclusions from those transition metal/MgO(100) studies still remain to be verified for other metal systems.

Ca is different from transition metals in terms of electronegativity and electronic configuration. It is also one of the main impurities in MgO and segregates to the surface upon annealing.[28] Recently, Zhu *et al.*[29] measured the adsorption heat of Ca adatoms deposited on MgO(100). They found that Ca has a large initial adsorption energy (450 KJ/mol), which rapidly drops to the bulk Ca cohesion energy (170 KJ/mol) as the Ca coverage increases to a monolayer.[29] Theoretical studies of Ca adsorption on the MgO(100) surface have not been systematically carried out [except for some first principles calculations of Ca segregation or doping on the MgO(100) surface[9,30]]. Using Ca to probe the MgO(100) surface can help provide additional information about the MgO(100) surface, which might be missed by only studying transition metal adsorption. The determination of the binding sites can help rationalize experimentally measured energetics. A related question is whether there is a single defect site that dominates the binding with any metal adatom or if different metals have different types of defects as nucleation centers. This will be part of the
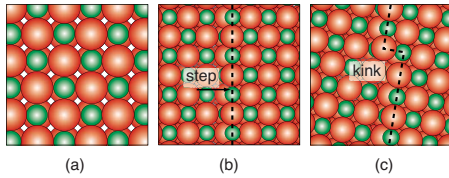
FIG. 1. (Color online) Models of MgO(100): top view of the (a) terrace, (b) step, and (c) kink. (Large red spheres are O atoms and small green spheres are Mg.)

topics to be addressed in this work. Our collaboration with Zhu *et al.*[29] has led to some interesting discovery about both the interface and the MgO(100) surface itself. In this work, we provide more details about the theoretical aspect of the Ca/MgO studies.

II. CALCULATION METHODOLOGY

DFT calculations are performed with the Vienna *ab initio* simulation package (VASP) by using the PW91 functional[31] and projector augmented wave based pseudopotentials.[32] A plane wave cutoff of 250 eV, which is appropriate for the pseudopotentials, is used with a $2 \times 2 \times 1$ Monkhorst–Pack sampling of the Brillouin zone. Spin polarization is checked and applied whenever it is necessary. Geometry optimizations are considered converged when the maximum force on each atom drops below 0.001 eV/Å.

The MgO(100) substrate is modeled as a three-layer slab with 36 atoms in each layer. The simulation box dimensions are $12.7 \times 12.7 \times 16.7$ Å^3. Figure 1(a) shows the MgO(100) substrate. The lower two layers of the substrate are held frozen at the optimal DFT lattice constant of 4.23 Å, which compares well with the 4.21 Å experimental lattice constant. Larger boxes with four MgO(100) layers are used for step $(15.0 \times 12.7 \times 20.5$ Å$^3)$, kink cells $(13.1 \times 15.0 \times 25.5$ Å$^3)$, and some large clusters $(16.9 \times 16.9 \times 16.9$ Å$^3)$. The substrates with step sites are built by tilting the slab [Fig. 1(b)] with the bottom layer frozen during geometry optimizations. The substrates with kink sites are built by either tilting the slab or adding a row of atoms to the step edge [Fig. 1(c)]. Figure 2 illustrates three types of point defects that are considered in this study.

A Bader *atoms-in-molecules* charge analysis[33] is conducted by using a grid-based algorithm.[34,35] The "charge transfer" for an atom refers to the change of its Bader charge relative to the neutral atom. Diffusion barriers are calculated with the nudged elastic band (NEB) method.[36,37]
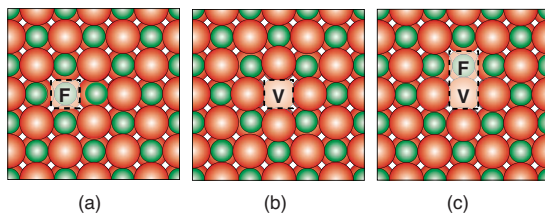
FIG. 2. (Color online) Models of point defects: (a) an O vacancy, F-center, (b) a Mg vacancy, V-center; and (c) a divacancy formed by removing a Mg-O pair.
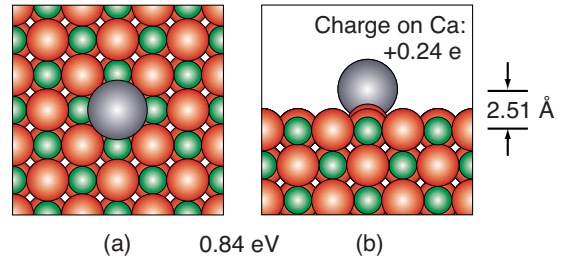
FIG. 3. (Color online) Ca monomer at an O site: (a) top view and (b) side view. (The largest gray circle is Ca.)

Adsorption energies, E_{ads}, for a cluster of n Ca atoms on the MgO surface are calculated as

$$-E_{ads} = E_{sys} - nE_{Ca} - E_{MgO}, \qquad (1)$$

where E_{sys} is the energy of n Ca atoms adsorbed on the MgO surface, E_{Ca} is the energy of an isolated gas phase Ca atom, and E_{MgO} is the energy of the MgO substrate. In the adsorption of an oxygen adatom or molecule, the reference energy E_{O_2} is that of the gas phase oxygen molecule for the same amount of oxygen atoms.

III. Ca ADSORPTION ON THE TERRACE

A. Monomer

The Ca monomer adsorbs on top of an O anion on the flat MgO(100) surface (terrace), similar to other metal adatoms, including Cu, Pd, Ag, and Ni.[38–40] The adsorption energy is 0.84 eV and the distance between the Ca and O atoms is 2.51 Å (Fig. 3). A Bader charge analysis shows that the Ca monomer carries a positive net charge of 0.24e, which indicates that charge is transferred from Ca to the surface. Upon adsorption, the O atom directly below the Ca monomer rises upward by 0.3 Å relative to the other surface atoms. The electronic ground state is not spin polarized. Ca monomers diffuse by hopping between nearest-neighbor O sites with a barrier of 0.45 eV.

B. Dimer

To determine the effect of the Ca-substrate interaction on Ca-Ca bonding, we calculated the adsorption energy of several Ca dimer configurations (Fig. 4). Surprisingly, the adsorption energy of a dimer (D1) on two neighboring anion sites [Fig. 4(a)] is only 0.78 eV/atom, which is less than the monomer adsorption energy. The Ca dimer–surface distance
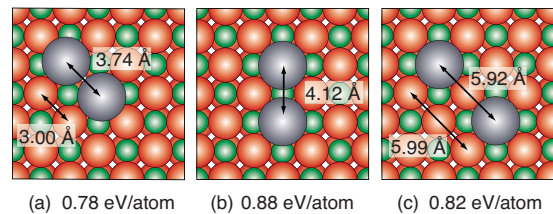
FIG. 4. (Color online) Ca dimer configurations with increasing separation distances. The optimal structure for the dimer is in next-nearest-neighbor sites (b).
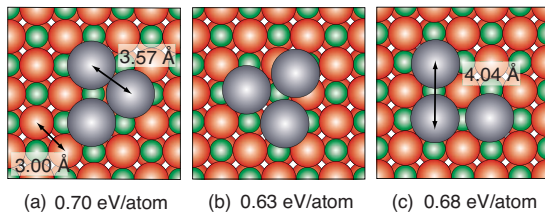
FIG. 5. (Color online) Ca trimer confirmations: (a) tilted flat triangle, (b) tilted triangle, and (c) expanded triangle.

of 2.51 Å is the same as that for the monomer. The Ca-Ca bond length is 0.7 Å longer than the O-O distance in the MgO substrate, while the epitaxial Ca-Ca distance (3.74 Å) is smaller than the gas phase dimer bond length of 4.13 Å. A stretched dimer (D2) with Ca atoms on next-nearest-neighbor O sites is slightly more stable [Fig. 4(b)], just as stable as two adsorbed monomers. When the separation distance is further increased, the dimer essentially dissociates into two monomers [Fig. 4(c)]. The vertical Ca dimer (0.58 eV/ atom) is less stable than epitaxial structures. A Bader analysis shows that each of the D1 dimer atoms carries a positive charge of $0.2e$.

The most stable dimer (D2) can transform into the unstable dimer (D) by crossing a barrier of 0.5 eV, while the reverse process has a barrier of 0.3 eV. Transitions between D1 and D3 (two monomers) have barriers of about 0.3 eV. Thus, the Ca dimer can either diffuse or dissociate on the terrace in a time scale of microseconds at room temperature.

C. Trimer

The most stable trimer configuration is a tilted triangle, as shown in Fig. 5(a), which has an adsorption energy of 0.70 eV/atom. Only the linear flat trimer (0.52 eV/atom, not shown here) is spin polarized (magnetization: 1.0); all triangle trimers are not spin polarized. A Bader analysis shows that each of the trimer atoms carries a positive charge of $0.2e$. Each of these trimers is unstable as compared to three isolated monomers on the terrace.

D. Tetramer

Three tetramer geometries are compared in Fig. 6: a three-dimensional (3D) tetrahedron and two two-dimensional (2D) planar squares. The adsorption energy is almost the same (~1.0 eV/atom) for the tetrahedron [Fig. 6(a)] and the compact planar clusters [Fig. 6(b)]. Both of these structures are slightly more stable than the expanded square tetramer [Fig. 6(c)] and the tilted tetrahedron [Fig. 6(d)]. Only the ex-

(a)0.98 eV/atom (b)0.97 eV/atom (c)0.93 eV/atom (d)0.96 eV/atom
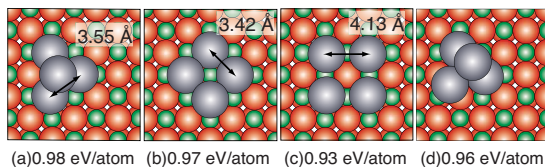
FIG. 6. (Color online) Ca tetramers: (a) tetrahedron, (b) compact square, (c) expanded square, and (d) tilted tetrahedron.
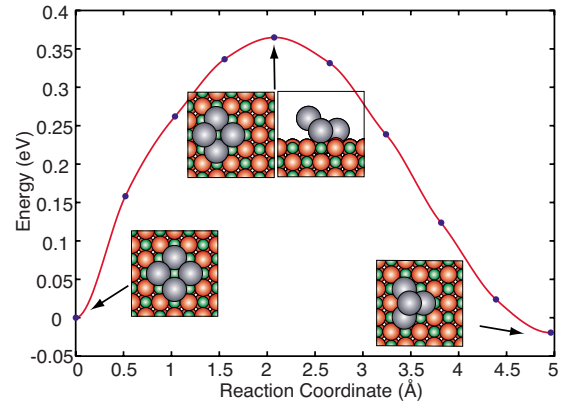
FIG. 7. (Color online) The transition of a 2D tetramer to a 3D tetrahedron. Both top and side views of the saddle point are presented.

panded tetramer shows a small spin polarization (magnetization: 0.5) in the electronic ground state. A Bader analysis shows that each of the tetramer atoms in direct contact to the surface carries a positive charge of $0.3e$. The tetrahedron is 0.4 eV more stable than two dimers—0.56 eV more stable than four monomers on the terrace.

The transition between the flat square tetramer and the tetrahedron occurs via a simple one-step process with a barrier of 0.36 eV (see Fig. 7). The tetrahedron can diffuse through a rollover mechanism, similar to the Pd tetrahedron on Mg(100),[41] but, here, there is an intermediate state [Fig. 6(d)] in the diffusion pathway, as shown in Fig. 8. The barrier for a tetrahedron to diffuse on the surface is only 0.12 eV, which is much lower than monomer diffusion.

E. Pentamer

The pyramidal pentamer was found to favor a three-dimensional structure, as shown in Fig. 9(a). The Ca pentamer has an adsorption energy of 1.1 eV/atom, which is significantly larger than the monomer binding energy (0.84 eV/atom). A flat "q-shape" pentamer [Fig. 9(b)] is less stable (0.97 eV/atom). The transformation of a flat pentamer into a pyramidal one is either a two-step process with a bar-
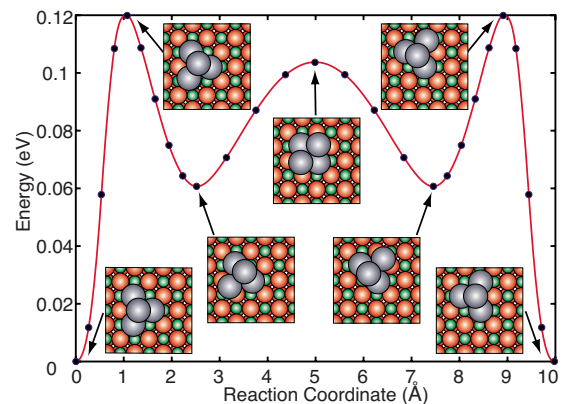
FIG. 8. (Color online) The Ca tetrahedron diffuses via a rollover mechanism.

(a) 1.13 eV/atom   (b) 0.97 eV/atom   (c) 0.91 eV/atom
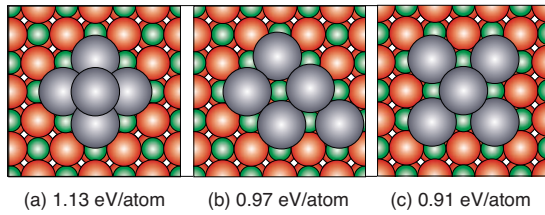
FIG. 9. (Color online) Ca pentamers: (a) pyramidal, (b) flat "q" shape, and (c) flat square.

rier of 0.13 eV or a one-step jump-up process with a barrier of 0.3 eV (Fig. 10).

F. Larger clusters

In order to calculate the structure and binding energy of larger clusters, we used a large MgO(100) substrate with 64 atoms on each of three layers, for which a Γ-point sampling of the Brillouin zone was found to be sufficient. A nine-atom two-dimensional island can form a compact island on the terrace [see Fig. 11(a)] with an adsorption energy of 1.01 eV/atom. The same nine atoms can also form a larger 2D island with every other oxygen site occupied [see Fig. 11(b)] with an adsorption energy of 1.1 eV/atom. The three-dimensional two-layer structures shown in Figs. 11(c) and 11(d) adsorb with 1.18 and 1.14 eV/atom, respectively. These results show that three-dimensional Ca islands are more stable than two-dimensional structures

G. Overlayers

A planar half-monolayer is formed by putting Ca atoms on every other oxygen site on the surface [Fig. 12(a)], with an adsorption energy of 1.27 eV/atom. When the Ca coverage reaches one monolayer, the repulsion between Ca atoms on nearest-neighbor oxygen sites pushes half of the Ca atoms upward. The resulting bilayer structure [see Figs. 12(b) and 12(c)] is bound with 1.61 eV/atom, which approaches the cohesive energy of bulk Ca (1.83 eV/atom). The monolayer
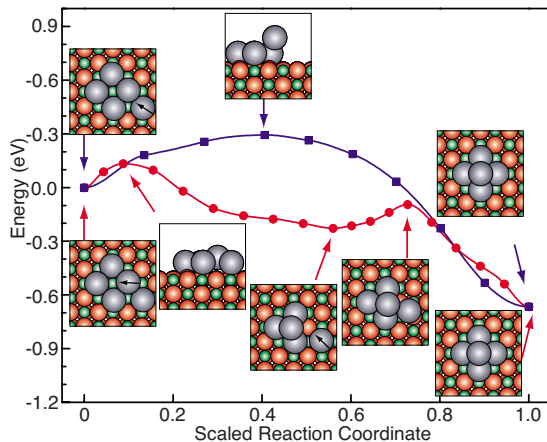
FIG. 10. (Color online) The transition of a flat q-shape pentamer into a pyramid. The total displacement for the two-step (lower red) path is 9.1 Å and is 7.6 Å for the one-step (upper blue) path.

(a)1.01 eV/atom(b)1.10 eV/atom(c)1.18 eV/atom(d)1.14 eV/atom
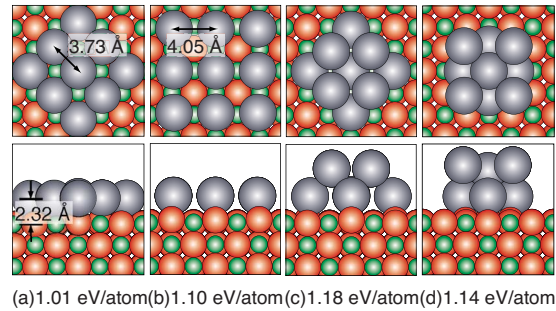
FIG. 11. (Color online) Nine-atom Ca clusters (coverage of 9/32 ML): (a) a compact 2D island, (b) an expanded 2D island, (c) 3D clusters, and (d) a compact 3D cluster.

shows no spin polarization. A Bader analysis shows that the charge transfer between Ca and MgO in the monolayer coverage is small ($\sim 0.15e$/atom).

IV. Ca ADSORPTION ON POINT DEFECTS

A. Monomer on a F center

A F center is created by removing a neutral oxygen atom from the surface [Fig. 2(a)]. Figure 13(b) shows that a Ca monomer binds above the F center instead of occupying the vacancy site. The weak binding energy (0.36 eV) and the negligible charge transfer between Ca and the substrate are indicative of a weak interaction between the Ca atom and the Mg cations surrounding the vacancy. The adsorption energy of Ca on a positively charged F^+ center is 0.76 eV, which is twice as strong as on a neutral F center [Fig. 13(c)]. Only the F^+ center binds Ca with spin polarization (magnetization: 0.9). A Bader analysis shows that the F^+ center traps $0.4e$ before the adsorption of Ca, and $0.6e$ after that; the net charge on the Ca is $+0.23e$.

B. Monomer in a V center

Since F-type centers do not bind Ca monomers more strongly than on the terrace, it is interesting to see if there are other types of defect sites that can serve as anchoring sites for Ca adatoms. The V center defect is created by removing a Mg atom from the surface [Fig. 2(b)]. An adsorbed Ca atom binds strongly to the defect (10.7 eV), almost perfectly replacing the missing Mg atom [Figs. 14(a) and 14(b)]. The net charge on Ca is $+1.5e$, which is close to the net charge on Mg in the substrate ($+1.7e$),[42] while the Mg vacancy does not trap electrons. When a second gas-phase Ca atom binds

(a) 1.27 eV/atom   (b)   1.61 eV/atom   (c)
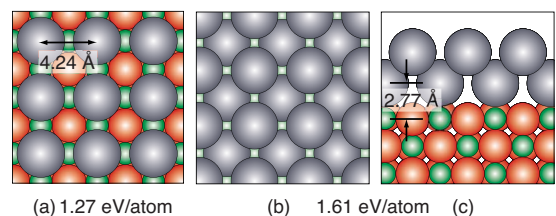
FIG. 12. (Color online) Ca (a) half-monolayer and [(b) top view and (c) side view] full monolayer.

(a) top view　　(b) 0.36 eV / atom　　(c) 0.76 eV / atom
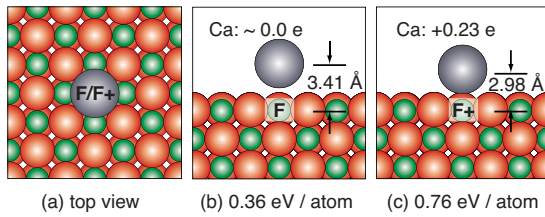
FIG. 13. (Color online) Ca monomers at F-type vacancy sites: (a) top view, (b) side view of the F center, and (c) side view of the F$^+$ center.

to the one already in the V center, 0.5 eV is released. The interaction between these Ca atoms is therefore repulsive since the second monomer binds more strongly on the terrace (0.84 eV).

A divacancy is created when a Mg-O pair is removed from the surface [Fig. 2(c)]. This type of vacancy has been found to strongly bind transition metals such as Pt (Ref. 16) and Pd.[26] Our calculation confirms this; Ca binds on a divacancy with an adsorption energy of 5.54 eV. Here, the Ca monomer goes into the substrate and substitutes for the missing Mg ion [Figs. 14(c) and 14(d)]. The charge transfer from Ca to the substrate is significant (1.4e), while the electronic state shows no spin polarization. Once the V center is filled, a second Ca atom binds weakly to the remaining F center, with a binding energy of 0.4 eV.

V. STEPS

A. Monomer

Steps are expected to be prevalent on the MgO surface. The Ca monomer adsorbs at the O step site by making two Ca-O bonds one to an O in the step and one below on the terrace [Figs. 15(a) and 15(b)]. The binding energy of 2.11 eV is therefore much stronger than on the terrace (0.85 eV). The charge transfer from Ca to the surface is 0.55e and the electronic states show no spin polarization. The Ca adatom does not bind to a Mg step site.

The mobility of Ca monomers along the step is also investigated with the NEB method. We find that the Ca monomer does not readily diffuse along the step. Instead, it must first leave the step by crossing a barrier of 1.4 eV to an intermediate state, which is an oxygen site near the step, as shown in Fig. 15(c). Then it hops back to the step. The process can continue via a zigzag path, as shown in Fig. 15(b). The high diffusion barrier means that steps trap and immobilize Ca monomers at low temperature.

(a)　10.7 eV　(b)　　　　(c)　5.54 eV　(d)
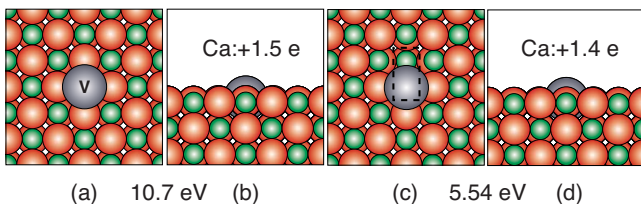
FIG. 14. (Color online) Ca monomer at V-type vacancy sites: a V center [(a) top and (b) side views] and a divacancy center [(c) top and (d) side views].

(a)　　2.11 eV　(b)　　　　(c)　0.90 eV
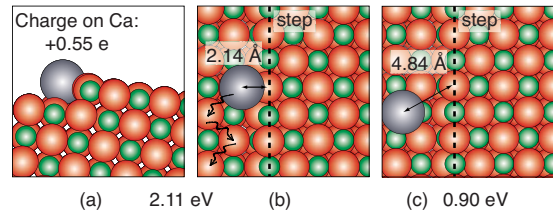
FIG. 15. (Color online) The Ca monomer at a step: (a) side view and (b) top view. The Ca atom binds to an O atom in the step and another on the terrace. The Ca atom diffuses along the step via a terrace O site (wiggly arrows). The intermediate state is shown in (c).

B. More atoms on the step

As more Ca adatoms bind to the step, the adsorption energy per atom does not change significantly. Figure 16 shows how the atoms bind at oxygen sites along the step; the Ca-Ca interaction between adjacent O step sites is slightly attractive. Our calculations also show that Ca adatoms fill up the step edges first, because the adsorption of one Ca adatom on the oxygen site near the step [Fig. 15(c)] gives off almost the same heat as on the terrace. On the other hand, the adsorption of a Ca adatom to a dimer occupying two edge sites [see Fig. 16(c)] releases 1.0 eV, which is 0.2 eV more than on the terrace. Adding one more Ca atom to make a tetramer on the step [Fig. 16(d)] gives off 1.14 eV. This relects the increasing stability as clusters grow at step edges.

C. Work function

Metal adsorption on the oxide surface involves a charge transfer between the adsorbate and the surface, which is related to the change in work function. Figure 17 shows that the Fermi level of the surface containing a step rises up by almost 1.8 eV upon the adsorption of the Ca monomer. Given almost the same average electrostatic potential before and after the adsorption (see Fig. 17), this suggests that charge flows from Ca to the surface to increase the Fermi level of the surface. A Bader charge analysis confirms this trend, which shows a charge transfer from Ca to the MgO surface in the amount of 0.6e.

D. Point defects at steps

There can be point defects on the step edges just as there are point defects on the MgO terrace. The binding of a Ca monomer on the possible point defects at the step edge is shown in Fig. 18. The monomer prefers to bind near the oxygen vacancy at the step edge with the adsorption energy

(a)2.09 eV/atom(b)2.32 eV/atom(c)1.74 eV/atom(d)1.59 eV/atom
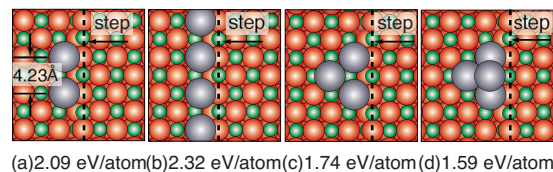
FIG. 16. (Color online) Ca atoms bound to a step, (a) dimer, (b) row, (c) trimer, and (d) tetramer.
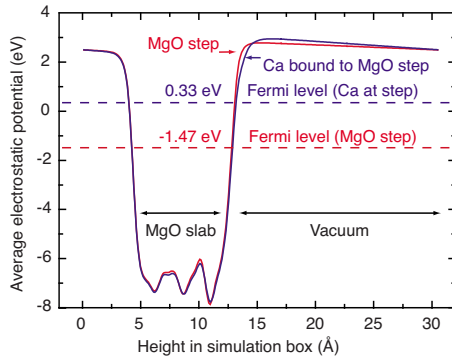
FIG. 17. (Color online) Electrostatic potential of a MgO step, before and after the adsorption of a Ca monomer. The increase of the Fermi level is consistent with the Bader analysis showing charge transfer from the Ca atoms to the substrate.

of 1.3 eV [Fig. 18(a)], which is weaker than the binding (2.1 eV) near the perfect step edge. This shows the same trend as compared to the oxygen vacancy on the terrace: Ca does not occupy the vacancy and only binds weakly to it. It also shows spin polarization (magnetization: 1.7). On the other hand, Ca adatoms occupy the Mg vacancies, binding strongly, as shown in Fig. 18(b). The adsorption energy is 9.8 eV, just a little bit less than the adsorption in the Mg vacancy on the flat area.

E. Role of oxygen at steps

MgO substrates are prepared by either cleaving the MgO crystal or oxidizing Mg in an oxygen environment. When the surface forms through oxidation, residual oxygen could be present before and during Ca adsorption experiments and, therefore, influence the heat of adsorption. Di Valentin *et al.*[43] calculated the structure of peroxo groups on regular and low-coordinated sites of MgO, BaO, etc. In this section, we first take a look at possible adsorption geometries and energies of oxygen atoms and molecules on the step, and then show how oxygen-decorated steps can affect Ca adsorption.

(a) 1.3 eV   (b) 9.8 eV
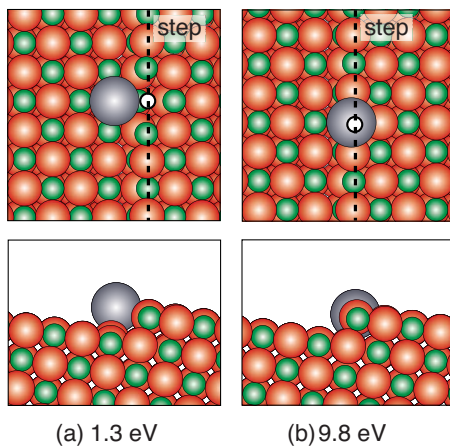
FIG. 18. (Color online) The Ca monomer adsorbs at point defects (white circles) on MgO(100) step edges: (a) an O vacancy and (b) a Mg vacancy.

(a) -0.87 eV   (b) 0.28 eV   (c) 0.19 eV/atom
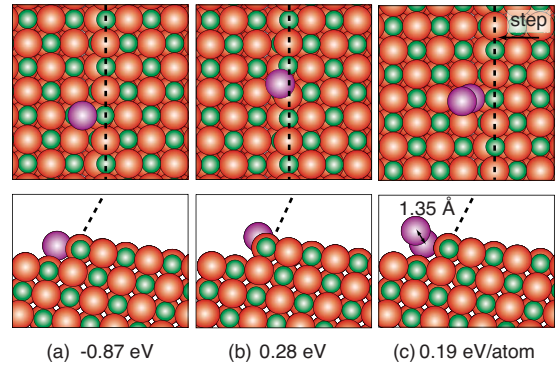
FIG. 19. (Color online) O adatoms (pink) adsorb at a step: (a) an O atom at a Mg step site, (b) an O atom forming a covalent bond with an O atom in the step, and (c) an O_2 molecule at a Mg step site.

A single oxygen atom can adsorb at a Mg step site as shown in Fig. 19(a) with an adsorption energy of −0.87 eV relative to half of the energy of a gas-phase O_2 molecule. The adsorption of a Ca adatom near it releases 8.1 eV [see Fig. 20(b)]. However, the O adsorption energy is negative (−0.87 eV), which indicates that O atoms would rather form O_2 molecules in the gas phase than adsorb on the step as O monomers.

Oxygen can also form a covalent bond to an existing O atom in the step as shown in Fig. 19(b). This is consistent with previous theoretical work.[43] The binding energy (0.28 eV) is favorable with respect to gas-phase O_2. This is interesting because it means that steps could be decorated with covalently bound O atoms. When a Ca atom binds at this step, it spontaneously breaks the O-O bond to form a stable Ca-O pair at the step (Fig. 20), releasing 7.0 eV. As shown in Fig. 21, there is a low, 0.2 eV, barrier for an oxygen adatom near the step [see Fig. 19(a)] to jump up and form a covalent bond with the oxygen atom in the step [see Fig. 19(b)]. The reverse barrier is 1.4 eV.

Molecular O_2 has a strong bond that is difficult to break, so we have also considered the binding of O_2 at steps. Figure 19(c) shows a bound O_2 molecule standing up at a Mg step

(a)   (b) 7.0 eV
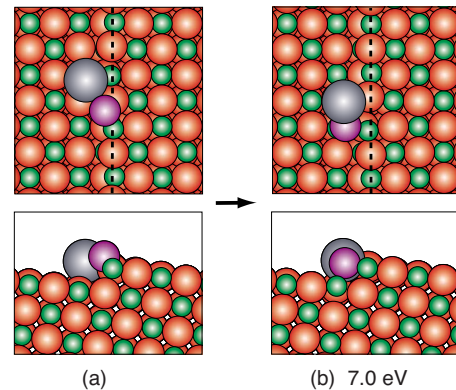
FIG. 20. (Color online) Addition of a Ca adatom breaks the O-step bond, which brings the covalently bound O (pink) into an adjacent step site: (a) Ca adatom near the O adatom on the step edge and (b) the optimized geometry. A lot of energy (7.0 eV) is released upon the adsorption of a Ca adatom.
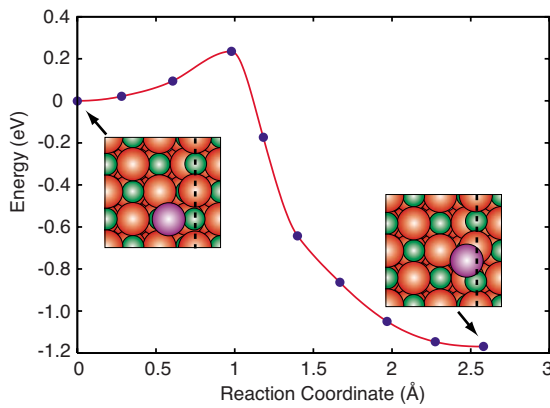
FIG. 21. (Color online) The oxygen adatom adsorbed against the step can easily be incorporated into the step. The dotted line shows the position of the step on the MgO(100) surface. The blue dots on the curve are the NEB images.

site. This structure maintains the strength of the O-O bond; it is only slightly stretched (1.35 Å) as compared to the gas phase (1.31 Å). It is also energetically stable, with an adsorption energy of 0.38 eV, relative to a gas phase O_2. This O_2 molecule does not dissociate on its own. The adsorption of a Ca adatom near this O_2-decorated step can release 7.4 eV [Fig. 22(a)]—significantly more than on the clean step (2.11 eV).

When a Ca adatom binds near a step-bound O_2 molecule, as shown in Fig. 22, the Ca adatom is most stabilized with the two oxygen atoms on each side along the step. Thermodynamically, Ca drives the dissociation of O_2 molecules adsorbed on the step and stabilizes both Ca and oxygen adsorbates on the step. The mechanism is surprising: the bottom oxygen adatom (pink) in Fig. 22(a) can pop out the oxygen in the step right next to the Ca adatom and form the structure of Fig. 22(b) (note that the colors on those two atoms have been switched); the barrier is only 1.1 eV. It further dissociates into the structure in Fig. 22(c). All three structures are quite stable.

Although the adsorption of oxygen atoms usually shows spin polarization, our calculations show that only the configuration in Fig. 19(a) is spin polarized. The oxygen incor-

porated in the step [Fig. 19(c)] shows no spin polarization, which is consistent with previous calculations.[43,44]
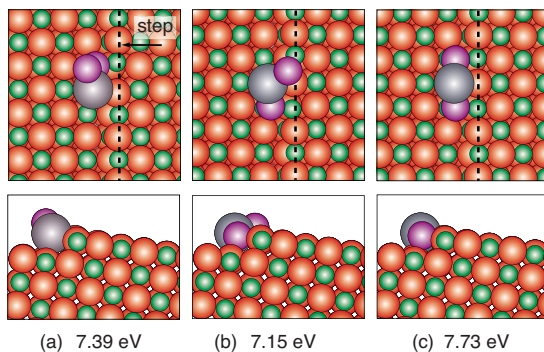
F. Vibrational modes of adsorbed oxygen at steps

As shown in the previous section, the oxygen atoms and molecules at steps could play a significant role for the binding of Ca adatoms on the step edges. Therefore, the validity of the oxygen existence on the step edge is a critical issue and should be verified through experiments. We calculated the vibrational frequency of oxygen molecule in the gas phase and found that the stretching mode has a frequency of 1100 cm^{-1}. Upon adsorption at steps in the configuration shown in Fig. 19(c), the stretching of the O-O bond blue-shifts to 1318 cm^{-1}. The oxygen stretching frequency stands alone from the MgO(100) vibrational modes [for thin films: <700 cm^{-1} (Ref. 45)] and therefore serves as a good probe target in experiments. There are also two soft modes for the same geometry: 84 and 90 cm^{-1}, which both involve molecular oxygen vibration without significantly stretching the O-O bond.

For the oxygen adatom incorporated in the step edge [Fig. 19(b)], there is one mode that is distinct from the vibrational modes of the MgO(100) substrate: 869 cm^{-1} for the adatom stretching along the bond between it and the nearest oxygen atom in the step. This is very close to the characteristic vibrational frequency of the peroxo group on the edge site calculated with a cluster model.[43] This strong mode can also be a target in studying the vibrational spectroscopy of the MgO(100) surface. There are also softer modes involving the wagging of the O- (O step) bond.[46]

G. Changes of density of states of oxygen adsorbates

Spectroscopic measurements, such as ultraviolet photo-emission spectroscopy (UPS), can show the emergence of new states by detecting electronic transitions. Our calculated density of states (DOS) data are plotted in Fig. 23. The adsorption of oxygen atoms introduces new states, especially in the energy region close to the Fermi level. These states can be determined with UPS to see if there are oxygen-decorated steps on the MgO(100) surface.

VI. KINKS

A. Monomer

We have also considered Ca binding at kink sites. Kink sites have lower coordinated atoms than steps or point defects. Our calculations show that a Ca monomer binds to the three O atoms at the kink site [Fig. 24(a)] with an adsorption energy of 3.9 eV. The charge transfer from Ca to the MgO surface is 1.14e. The electronic states show spin polarization (magnetization: 2.0). The Ca monomer does not bind at a Mg kink site. Instead, the Ca adatom moves to a nearby O site along the step with the adsorption energy of 2.8 eV, between the heat of adsorption on a kink and step site.

B. Larger Ca clusters

In order to model the growth of Ca clusters at steps and kink sites, we have added Ca adatoms near the kink site.

(a) 7.39 eV   (b) 7.15 eV   (c) 7.73 eV

FIG. 22. (Color online) Ca adatom adsorbs near two O (pink) adatoms at a step. (a) A standing O_2 molecule, (b) a stretched O_2 molecule, and (c) two O adatoms at adjacent Mg step sites. All energies are relative to a gas-phase O_2 molecule and Ca atom.
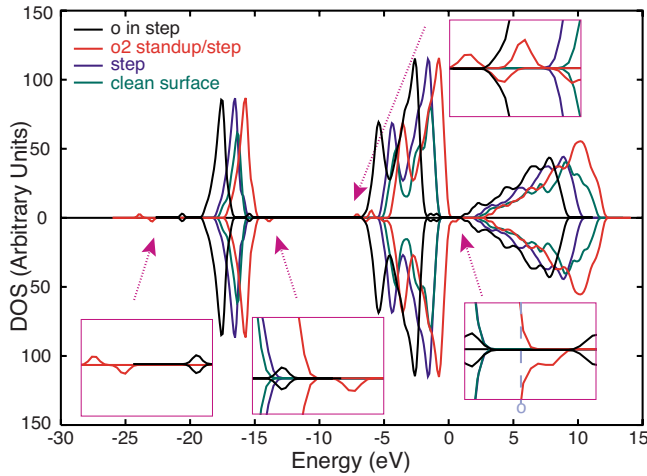
FIG. 23. (Color online) The density of states of MgO(100): (black) O atom incorporated in the step [Fig. 19(b)], (red) adsorbed with O$_2$ standing on the step [Fig. 19(c)], (blue) step [Fig. 1(b)], and (green) terrace [Fig. 1(a)] [Note: All (spin-up and spin-down) curves are shifted to align their Fermi energy levels to zero.]

Figures 24(b) and 24(c) show that the average adsorption energy per atom drops from 3.9 eV/atom (kink) to 3.17 and 2.87 eV/atom as more Ca adatoms land on the step next to the kink site. The adsorption of Ca atoms away from the kink sites is almost the same as the adsorption of Ca on the step.

VII. DISCUSSION

A. Adsorption of Ca on the MgO(100) terrace

DFT calculations show that Ca adatoms bind at oxygen sites on the terrace and diffuse by hopping over bridging hollow sites. This is consistent with the adsorption and diffusion of some transition metals on MgO(100).[39,47] The lower electron affinity of Ca, however, makes Ca adsorb differently from transition metals. The most significant difference is the charge transfer direction. Transition metals tend to accept a partial charge from the surface, specifically from the oxygen anion beneath.[17,47,48] On the other hand, Ca transfers charge to the surface, and this transferred charge is not localized on the oxygen anion beneath the Ca adatom. This charge transfer direction is verified by our work function calculation, which, in agreement with experimental measurements,[29] indicates a significant drop upon the adsorption of Ca. Our calculations also suggest that a greater charge transfer leads to a stronger binding (see Fig. 25).
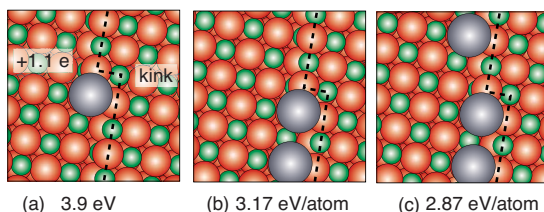
FIG. 24. (Color online) Ca adatoms on an O kink site: (a) monomer, (b) two atoms, and (c) three atoms along the kink-step.
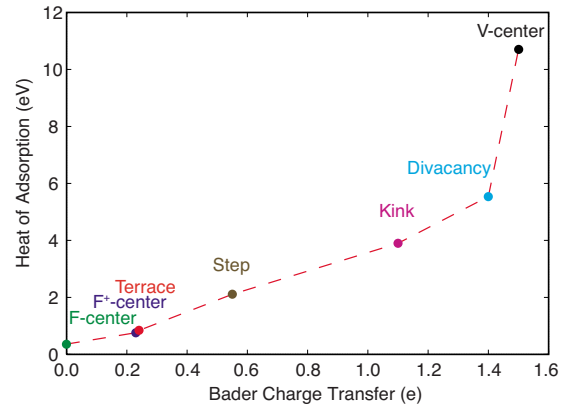
FIG. 25. (Color online) The correlation between the monomer adsorption energy and the Bader charge transfer from Ca to the surface.

The gas-phase Ca dimer has a large bond distance (4.13 Å), so that the epitaxial adsorption of a dimer [Fig. 4(a)] has internal strain and the adsorption heat is less than two separate monomers. A stretched dimer (D2) with Ca atoms on next-nearest-neighbor O sites is more stable [Fig. 4(b)]. This supports the claim that small metal clusters adsorbed on a MgO(100) surface tend to keep close to their gas-phase structure.[49] The most stable dimers are just 0.08 eV more stable than two monomers on the terrace. Even though dimers can diffuse around the surface (barrier: ~0.4 eV) at room temperature, our calculations show that the dissociation barrier is as low as the diffusion barrier. Therefore, Ca dimers will either dissociate into monomers or diffuse over the surface as rapidly as monomers. In either case, it is unlikely to form small clusters on the terrace at low deposition rates.

For larger clusters on the terrace, the Ca trimers are found to be 0.5 eV less stable than separate monomers. The most stable tetramer (tetrahedron) is 0.5 eV more stable than four Ca monomers, and it diffuses extremely fast (barrier: 0.12 eV), which is similar to Pd tetramer diffusion on MgO(100),[41] suggesting that the high mobility of small metal clusters on oxide terraces is generic. The pyramidal pentamer is 0.7 eV more stable than separate monomers. Larger clusters or islands are also stable. Therefore, there is a critical size for a Ca cluster to form on the terrace at room temperature (300 K): only a cluster as large as the tetramer is stable on the surface. Given the fact that small clusters are either unstable or very mobile on the terrace, even if the deposition flux is large enough to create some small clusters on the terrace, they are unlikely to form nucleation centers on the terrace. Other strong-binding sites such as point or extended defects will nucleate islands.

Our calculations also show that the transition from 2D clusters to 3D clusters on the terrace is rapid (barriers: 0.36 eV for tetramer and 0.3 eV for pentamer). Large 3D clusters are more stable than 2D islands. This implies that the island growth follows a 3D growth mode. Adatoms attaching to the island edges will easily climb up and form 3D structures.

TABLE I. The energy released by the adsorption of one Ca atom on a stable Ca cluster on layer on the surface. $E_{adh} = [E(Ca_{n+m}) - E(Ca_n) - E(Ca_{gas})]/m$.

Cluster $(n+m)$	Cluster (n)	E_{adh} (eV/atom)
Pentamer (5)	Tetrahedron (4)	1.7
ML (18)	Half ML(9)	1.9

B. Three-dimensional growth mode of Ca clusters

Our calculations show that Ca growth follows a 3D mode. The cohesion energy of bulk Ca has also been calculated with DFT and found to be 1.88 eV/atom, which is close to the experimental value of 1.83 eV/atom (177.8 kJ/mol).[50] In order to compare with the differential heat of adsorption from experiments, we calculated the heat released by one gas-phase Ca atom ending up on top of a Ca cluster on the terrace (through either landing or diffusion). The results presented in Table I show that the binding between a Ca adatom and a Ca overlayer is close to the Ca cohesion energy. Experimental measurements show that the energy released when a gas-phase Ca atom lands on a surface covered with Ca at half monolayer coverage is 1.75 eV/atom (170 kJ/mol).[29] This value is also close to the cohesion energy in bulk Ca. Provided that the defects on the surface are saturated, those Ca adatoms bind to existing islands. The energetics from DFT calculations is consistent with experiments in support of a 3D growth mode.[29]

C. Role of surface defects on Ca growth

We have concluded that the Ca islands form at undercoordinated defect sites, where Ca adatoms adsorb strongly. Point defects are probably the most abundant on MgO(100).[19] Surface oxygen point defects (both F and F$^+$ centers) do not bind Ca strongly enough to trap diffusing monomers. Ca has two valence electrons, but the F and F$^+$ centers will not accept more than one. Therefore, Ca monomers will continue to diffuse until they find a stronger binding site, such as Mg vacancies, Mg-O divacancies, steps, kinks or other extended defects. The Mg vacancies and divacancies bind Ca monomers very strongly since Ca adatoms fill in the anion vacancies; these defects could serve as anchoring sites. However, our calculations show that once the vacancy is filled with a Ca monomer, it will not bind another Ca adatom as strongly. Therefore, Mg-type vacancies capture Ca monomers and become similar to regular Mg sites on the terrace. EELS studies of MgO(100) growth on Ag(100) also suggested that Mg vacancies are not as abundant as O vacancies,[23] so it is reasonable to assume a low concentration of Mg vacancies.

Step and kink sites are intrinsic on an imperfect MgO(100) surface.[19,21] Our DFT calculations show that Ca monomers strongly bind at steps (2.11 eV) and do not easily diffuse along or away from the step edge (barrier: 1.4 eV). Therefore, Ca atoms that encounter a step will be captured. Kink sites bind Ca monomers more strongly (3.9 eV). There-

fore, both steps and kinks on the MgO(100) surface are anchoring sites for Ca nucleation and growth. As more Ca adatoms land on the surface, Ca islands expand to the terrace after filling the step rows, which release a reduced adsorption energy per atom, eventually reaching the Ca bulk heat of adsorption.

D. Two-state growth model

We have fitted a simple two-state growth model to the experimental differential heat of adsorption curves for Ca on MgO(100).[29] Briefly, in the two-state model, the Ca adatoms are mobile on the surface and, therefore, occupy those strong-binding defect sites first. The ratio between those strong-binding defects determines the initial heat of adsorption. With more Ca adatoms landing on the surface, 3D Ca islands grow at those defect sites. There is also a competition between seeking out unoccupied strong-binding sites and attaching to the Ca islands already formed around defects, but our calculations show that it is favorable to seek out the strong-binding sites when the cluster size is small (less than a pentamer). Then, other incoming Ca adatoms can either directly land on the existence big islands or merge in by diffusion and climb up to form 3D structures. In this regime, the adsorption heat is close to the cohesion energy of bulk Ca.

E. Comparison with experimental heats of adsorption

By comparing these DFT results with experimental heat of adsorption measurements, we hope to rationalize the observations and help identify the surface defects present on MgO. Experiments show that the first Ca adatoms bind very strongly to some intrinsic defect sites with a very large adsorption energy of 4.22 eV/atom (410 kJ/mol).[29] This value falls between our calculated adsorption energy of a Ca monomer on a kink site (3.92 eV/atom) and on a divacancy (5.54 eV/atom). Based on our calculations, we rule out the possibility that the F center (neutral or charged) is the intrinsic defect that strongly binds the initially deposited Ca monomers since Ca atoms weakly bind on F centers. If Ca clusters grow around steps and kinks, the initial adsorption energies will be weighted averages of 2.1 and 3.9 eV. That would create some discrepancy between DFT calculations and experimental measurements of the initial adsorption heat. The existence and population of Mg vacancy sites are still an open question. If there are Mg vacancies on the step edges, they would bind Ca adatoms as on the terrace: a Ca monomer fills in the vacancy, which releases about 10 eV. The presence of Mg vacancies would bring the initial heat of adsorption closer to the experimental value, but our calculations also show that additional Ca adatoms do not show a strong binding on Ca-filled Mg-type vacancies. However, the real surface is more complicated than our simple model, so it is reasonable to assume the existence of other types of strong binding defects[51] other than Mg vacancies.

The MgO substrate was prepared by the oxidation of Mg, followed by pumping out O$_2$ gas,[29] so it is reasonable to check if the oxygen molecules or atoms remain on the surface. Our calculations show that oxygen molecules can ad-
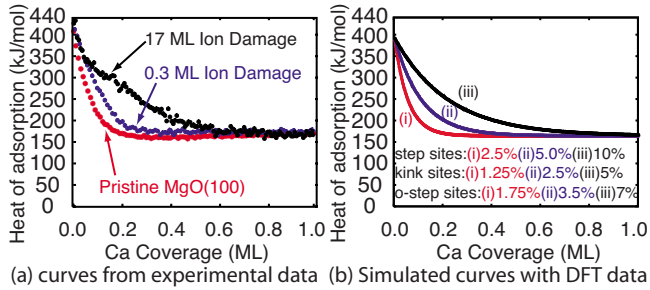
FIG. 26. (Color online) Simulation of two-state growth of Ca on MgO(100): Ca either binds to an unoccupied strong-binding site [as indicated in (b)] or forms a 3D island around the occupied defects with the binding energy of 1.7 eV/atom. All the heats of adsorption are differential. The experimental data (a) were taken from Ref. 29.

sorb on the step site, which are bound by 0.4 eV per molecule [Fig. 19(c)]. This opens up the possibility of oxygen-decorated steps, as suggested by previous DFT studies of peroxo groups.[43]

We have shown that oxygen atoms can form covalent bonds with the oxygen atoms in the step [Fig. 19(b)]. This is equivalent to an O_2 molecule filling in an oxygen vacancy on a step edge. That structure shows a binding energy of 0.3 eV relative to half of the O_2 gas-phase bond energy (i.e., more stable than molecular adsorption). This structure has a dissociation barrier of 1.4 eV, which means that an oxygen incorporated into the step is stable up to 600 K on a time scale of seconds. This temperature is typical of the annealing used in the preparation of MgO substrates. The adsorption of a nearby Ca adatom releases 7.0 eV. This high heat of adsorption, together with the adsorption energy on steps and kinks, brings the weighted average of the initial adsorption heat close to the experimental values.

Di Valentin *et al.* calculated the peroxo stretching frequencies on a series of oxides and compared them favorably to the experimental report about peroxo on BaO.[43,52,53] However, the existence of those oxygen-decorated steps on MgO still needs to be checked by experiments. Other possible strong binding sites can also be present,[51] but the generic two-state growth model will not be affected, except for a change in the initial heat of adsorption.

By using the two-state model, we simulated the heat of adsorption for Ca growth, considering only strong binding sites, as described in Ref. 29. With the introduction of oxygen-decorated step sites, the simulation curves agree well with experiment (Fig. 26).

If the surface is sputtered with Ar$^+$ as described in Ref. 29, additional oxygen vacancies, steps and kinks, magnesium vacancy or divacancy sites, or even some larger damaged regions will be created. The roles of those sites in Ca growth have been discussed in the previous paragraphs and the two-state 3D growth mode should still hold, because small Ca clusters are not easy to form on the terrace at room temperature. However, the effects of Ar$^+$ sputtering on the MgO(100) surface are still not fully understood; our assumption about the damaged surface should be taken with some caution. The nearly constant initial heat of adsorption observed in experiments before and after heavy surface damage[29] suggests either that there are no additionally created stronger-binding defect sites (e.g., only F-type centers are created) or that the ratio of the strong-binding defect sites is maintained.

The heats of adsorption for Ca adatoms on different binding sites on the MgO(100) surface are summarized in Table II.

TABLE II. Comparison of experimental Ca adsorption energies with the most likely DFT binding site.

Cluster/Site	DFT adsorption energy (eV/atom)
Monomer/O step	7.0
Monomer/O_2/step	7.4
Monomer/kink	3.9
Dimer/kink	3.2
Row/step	2.3
Monomer/step	2.1
3D island/terrace	$\geqslant 1.1$
2D island/terrace	$\geqslant 1.3$
Monolayer/terrace	$\geqslant 1.6$
Monomer/terrace	0.84

F. Metal adsorption to probe the role of defects

The uncertainty in the density of surface defects makes it difficult to unambiguously understand metal growth on the MgO(100) surface. The oxygen vacancy is thought of as the dominant vacancy on the surface.[21,26] Some transition metals, such as Pd and Au, have been found to nucleate and grow at oxygen vacancy sites.[22,27,54] This Ca/MgO(100) study does not rule out the existence of populous oxygen vacancy sites. The key point is that Ca adatoms do not bind strongly at F centers and will diffuse to other strong-binding intrinsic defects such as steps or kinks. If the metal binds strongly at oxygen vacancies, the growth mode will be dominated by the nucleation around F centers instead of steps, just as for Pd growth on the MgO(100) surface.[22,27] Therefore, the dominant defect sites for metal growth on MgO(100) can be different depending on the deposited metals. It is possible that there could be several types of defects that are comparably weighted in the distribution. It depends on which metal "probe" is used in the studies of the surface.

VIII. CONCLUSION

By using DFT calculations of Ca adsorption on various sites on the MgO(100) surface, we have shown that Ca nucleates island and grows somewhat differently from transition metals on the same surface. Upon adsorption, charge flows from the metal to the surface. Our calculations also show that Ca grows in a 3D mode according to the two-state kinetics on the MgO(100) surface, which is in agreement with experiment. Homogeneous growth on the terrace is not favored due to the high mobility of small Ca clusters. The

adsorption sites that contribute most to the growth mode are steps, kinks, and, if possible, Mg-type vacancies and O_2-decorated steps. A mixture of those strong-binding sites on the surface can rationalize the experimental measurement of the initial adsorption heat. The population of oxygen vacancy on MgO(100) is not probed by Ca adsorption. The role of surface defects on the MgO(100) surface can significantly be different for different metals.

[1] C. R. Henry, Surf. Sci. Rep. **31**, 235 (1998).

[2] J. A. Venables, *Introduction to Surface and Thin Film Processes* (Cambridge University Press, Cambridge, England, 2000).

[3] H. J. Freund, M. Bäumer, and H. Kuhlenbeck, Adv. Catal. **45**, 333 (2000).

[4] M. Valden, X. Lai, and D. W. Goodman, Science **281**, 1647 (1998).

[5] M. Moseler, H. Hakkinen, and U. Landman, Phys. Rev. Lett. **89**, 176103 (2002).

[6] T. H. Lee and R. M. Dickson, Proc. Natl. Acad. Sci. U.S.A. **100**, 3043 (2003).

[7] C. Duriez, C. Chapon, C. R. Henry, and J. M. Rickard, Surf. Sci. **230**, 123 (1990).

[8] V. E. Henrich and P. A. Cox, *The Surface Science of Oxides* (Cambridge University Press, Cambridge, England, 1994).

[9] Y. Yan, M. F. Chisholm, S. J. Pennycook, and S. T. Pantelides, Surf. Sci. **442**, 251 (1999).

[10] C. T. Campbell, Surf. Sci. Rep. **27**, 1 (1997).

[11] C. T. Campbell and D. E. Starr, J. Am. Chem. Soc. **124**, 9212 (2002).

[12] G. Renaud, R. Lazzari, C. Revenant, A. Barbier, M. Noblet, O. Ulrich, F. Leroy, J. Jupille, Y. Borensztein, C. R. Henry, J. P. Deville, F. Scheurer, J. Mane-Mane, and O. Fruchart, Science **300**, 1416 (2003).

[13] N. López, F. Illas, N. Rösch, and G. Pacchioni, J. Chem. Phys. **110**, 4873 (1999).

[14] L. Giordano, J. Goniakowski, and G. Pacchioni, Phys. Rev. B **64**, 075417 (2001).

[15] A. Markovits, M. K. Skalli, C. Minot, G. Pacchioni, N. López, and F. Illas, J. Chem. Phys. **115**, 8172 (2001).

[16] A. Bogicevic and D. R. Jennison, Surf. Sci. Lett. **515**, L481 (2002).

[17] Y. F. Dong, S. J. Wang, Y. Y. Mi, Y. P. Feng, and A. C. H. Huan, Surf. Sci. **600**, 2154 (2006).

[18] G. Barcaro and A. Fortunelli, New J. Phys. **9**, 22 (2007).

[19] C. Barth and C. R. Henry, Phys. Rev. Lett. **91**, 196102 (2003).

[20] M. Chiesa, M. C. Paganini, E. Giamello, C. Di Valentin, and G. Pacchioni, Angew. Chem., Int. Ed. **42**, 1759 (2003).

[21] G. Haas, A. Menck, H. Brune, J. V. Barth, J. A. Venables, and K. Kern, Phys. Rev. B **61**, 11105 (2000).

[22] J. A. Venables, L. Giordano, and J. H. Harding, J. Phys.: Condens. Matter **18**, S411 (2006).

[23] J. Kramer, W. Ernst, C. Tegenkamp, and H. Pfnür, Surf. Sci. **517**, 87 (2002).

[24] M. Sterrer, E. Fischbach, T. Risse, and H. J. Freund, Phys. Rev. Lett. **94**, 186101 (2005).

[25] A. M. Ferrari and G. Pacchioni, J. Phys. Chem. **99**, 17010 (1995).

[26] L. Giordano, C. Di Valentin, J. Goniakowski, and G. Pacchioni, Phys. Rev. Lett. **92**, 096105 (2004).

[27] L. Xu, C. T. Campbell, H. Jónsson, and G. Henkelman, Surf. Sci. **601**, 3133 (2007).

[28] R. C. McCune and P. Wynblatt, J. Am. Ceram. Soc. **66**, 111 (1983).

[29] J. Zhu, J. A. Farmer, N. Ruzycki, L. Xu, C. T. Campbell, and G. Henkelman, J. Am. Chem. Soc. **130**, 2314 (2008).

[30] A. L. Almeida, J. B. L. Martins, E. Longo, N. C. Furtado, C. A. Taft, J. R. Sambrano, and J. W. A. Lester, Int. J. Quantum Chem. **84**, 705 (2001).

[31] J. P. Perdew, in *Electronic Structure of Solids*, edited by P. Ziesche and H. Eschrig (Akademie Verlag, Berlin, 1991).

[32] G. Kresse and D. Joubert, Phys. Rev. B **59**, 1758 (1999).

[33] R. F. W. Bader, *Atoms in Molecules: A Quantum Theory* (Oxford University Press, New York, 1990).

[34] G. Henkelman, A. Arnaldsson, and H. Jónsson, Comput. Mater. Sci. **36**, 354 (2006).

[35] E. Sanville, S. D. Kenny, R. Smith, and G. Henkelman, J. Comput. Chem. **28**, 899 (2007).

[36] G. Henkelman, B. P. Uberuaga, and H. Jónsson, J. Chem. Phys. **113**, 9901 (2000).

[37] G. Henkelman and H. Jónsson, J. Chem. Phys. **113**, 9978 (2000).

[38] N. López and F. Illas, J. Phys. Chem. B **102**, 1430 (1998).

[39] A. Musolino, V. Selloni, and R. Car, J. Chem. Phys. **108**, 5044 (1998).

[40] A. V. Matveev, K. M. Neyman, G. Pacchioni, and N. Rösch, Chem. Phys. Lett. **299**, 603 (1999).

[41] L. Xu, G. Henkelman, C. T. Campbell, and H. Jónsson, Phys. Rev. Lett. **95**, 146103 (2005).

[42] G. Henkelman, B. P. Uberuaga, D. J. Harris, J. H. Harding, and N. L. Allan, Phys. Rev. B **72**, 115437 (2005).

[43] C. Di Valentin, R. Ferullo, R. Binda, and G. Pacchioni, Surf. Sci. **600**, 1147 (2006).

[44] G. Genestea, J. Morillo, and F. Finocchi, J. Chem. Phys. **122**, 174707 (2005).

[45] L. Savio, E. Celasco, L. Vattuone, M. Rocca, and P. Senet, Phys. Rev. B **67**, 075420 (2003).

[46] To watch the movies for those modes, please visit http://theory.cm.utexas.edu/camgo/

[47] L. Xu, G. Henkelman, C. T. Campbell, and H. Jónsson, Surf. Sci. **600**, 1351 (2006).

[48] J. R. B. Gomes, F. Illas, and B. Silvi, Chem. Phys. Lett. **388**, 132 (2004).

[49] A. M. Ferrari, C. Y. Xiao, K. M. Neyman, G. Pacchioni, and N.

Rösch, Phys. Chem. Chem. Phys. **1**, 4655 (1999).

[50] D. R. Lide, *CRC Handbook of Chemistry and Physics*, 87th ed. (CRC, New York, 2006).

[51] M. Chiesa, E. Giamello, C. Di Valentin, G. Pacchioni, Z. Sojka, and S. Van Doorslaer, J. Am. Chem. Soc. **127**, 16935 (2005).

[52] C. Hess and J. H. Lunsford, J. Phys. Chem. B **106**, 6358 (2002).

[53] M. Nakamura, H. Mitsuhashi, and N. Takezawa, J. Catal. **138**, 686 (1992).

[54] Z. Yan, S. Chinta, A. A. Mohamed, J. J. P. Fackler, and D. W. Goodman, J. Am. Chem. Soc. **127**, 1604 (2005).